Geophysical Research Letters

RESEARCH LETTER
10.1029/2022GL098704

Key Points:

- Secondary multi-phase processes dominate daytime HONO levels in aged (>3 hr) fire smoke
- The inferred strength of secondary HONO production is most correlated to NO_2, aerosol surface area, and particulate nitrate
- We find significantly weaker HONO formation from particulate nitrate photolysis than previous reports

Supporting Information:

Supporting Information may be found in the online version of this article.

Correspondence to:

J. A. Thornton,
joelt@uw.edu

Citation:

Peng, Q., Palm, B. B., Fredrickson, C. D., Lee, B. H., Hall, S. R., Ullmann, K., et al. (2022). Direct constraints on secondary HONO production in aged wildfire smoke from airborne measurements over the Western US. *Geophysical Research Letters*, *49*, e2022GL098704. https://doi.org/10.1029/2022GL098704

Received 16 MAR 2022
Accepted 30 JUL 2022

Direct Constraints on Secondary HONO Production in Aged Wildfire Smoke From Airborne Measurements Over the Western US

Qiaoyun Peng[1], Brett B. Palm[1,2], Carley D. Fredrickson[1], Ben H. Lee[1], Samuel R. Hall[2], Kirk Ullmann[2], Andrew J. Weinheimer[2], Ezra Levin[3], Paul DeMott[3], Lauren A. Garofalo[3], Matson A. Pothier[3], Delphine K. Farmer[3], Emily V. Fischer[4], and Joel A. Thornton[1]

[1]Department of Atmospheric Sciences, University of Washington, Seattle, WA, USA, [2]Atmospheric Chemistry Observations & Modeling Laboratory, National Center for Atmospheric Research, Boulder, CO, USA, [3]Department of Chemistry, Colorado State University, Fort Collins, CO, USA, [4]Department of Atmospheric Science, Colorado State University, Fort Collins, CO, USA

Abstract Nitrous acid (HONO) mixing ratios measured in aged wildfire smoke plumes were higher than expected from known homogeneous chemical reactions. In a representative smoke plume, intercepted hours to days downwind of the source, the missing HONO source was highly correlated to particulate nitrate photolysis and NO_2 reactive uptake to particles. Using a multilinear regression involving these two sources, we could explain the missing HONO production in this plume ($R^2 = 0.77$). The resulting fit parameters from this plume had good explanatory power ($R^2 = 0.64$) for missing HONO production in other fire plumes. The mean enhancement factor for particulate nitrate photolysis relative to gas-phase nitric acid photolysis was 63 and the mean NO_2 reactive uptake coefficient to submicron aerosol surface area forming HONO was 4.9×10^{-4}. Given the likelihood of other neglected secondary HONO sources, these values are upper-limits, suggesting a need to revisit HONO formation mechanisms in aged wildfire smoke.

Plain Language Summary A river of smoke from multiple wildfires was sampled far downwind and served as a natural laboratory for evaluating sources of nitrous acid (HONO) in aged wildfire smoke. HONO photolysis is an important source of reactive oxidants that initiate chemical transformations of wildfire emissions. We demonstrate that sources of HONO from chemical processes, known as secondary HONO sources, can largely be explained by two processes – the photolysis of particulate nitrate and the reactive uptake of nitrogen dioxide (NO_2) to smoke aerosol particles. High time resolution in situ observations of HONO and auxiliary measurements were used to map out variations in the missing HONO source across a wide span of wildfire characteristics. The results place an upper limit on the magnitude of HONO sources from particulate nitrate photolysis, and suggest that the heterogeneous NO_2 reactive uptake to smoke particles could be more important than previous field studies have indicated. These findings demonstrate the existence of additional processes other than direct emissions responsible for HONO formation in fire smoke. This secondary HONO source could increase the oxidizing capacity of wildfire smoke plumes significantly downwind of the emission source and therefore affect the formation and lifetime of other secondary wildfire smoke components.

1. Introduction

Nitrous acid (HONO) is an important precursor of the hydroxyl radical (OH), a key atmospheric oxidant. Wildfires are a major HONO source, including direct emissions and homogeneous reaction between nitrogen oxide (NO) and OH. In addition, secondary HONO formation pathways have been suggested in various environments (Bao et al., 2018; Z. Liu et al., 2014; K. Stemmler et al., 2007; Ye et al., 2016; Zhou et al., 2001). Recently, we showed for wildfires, HONO primary emissions either dominate over secondary sources or cannot easily be separated from fast secondary formation close to the fires (Peng et al., 2020). However, as smoke travels downwind, photolytic loss of directly emitted HONO (atmospheric e-folding lifetime $\tau \sim 0.3$ hr) implies that secondary HONO formation will become important to HONO in aged smoke plumes.

There is not yet consensus on the importance of secondary HONO sources and the dominant mechanisms are still widely debated. Field studies outside of wildfire plumes find daytime HONO levels higher than expected

from known reactions, with large unidentified HONO sources needed to reconcile such observations (Sörgel et al., 2011; Ye et al., 2018). In contrast, some studies find known pathways explain observed HONO without the need to invoke additional mechanisms (Neuman et al., 2016), or that the additional HONO sources may be an artifact of model assumptions or of measurement interferences (R. Crilley et al., 2016; B. H. Lee et al., 2013; Veres et al., 2015).

Heterogeneous reactions of NO_2 on surfaces are considered a potentially ubiquitous source of secondary HONO (R1). The importance of reactive uptake to aerosol particle surfaces is especially uncertain, with measured reactive uptake coefficients ($\gamma_{NO_2\rightarrow HONO}$) spanning 4 orders of magnitude from 10^{-7} to 10^{-3} (Acker et al., 2004; Ammann et al., 1998; Finlayson-Pitts et al., 2003; Gustafsson et al., 2008; Han et al., 2016; Kleffmann et al., 1999; Z. Liu et al., 2014; Monge et al., 2010; Stemmler et al., 2007). Photo-enhanced NO_2 heterogeneous chemistry via NO_2 hydrolytic disproportionation has also been reported (R2, George et al., 2005). Colussi et al. (2013) found that dicarboxylic acid anions may catalyze NO_2 to HONO conversion on aqueous aerosol surfaces with $\gamma_{NO_2\rightarrow HONO}$ ranging from 10^{-4} to 10^{-3}. Z. Liu et al. (2014) supported this hypothesis using correlation analysis to account for enhanced HONO formation in Beijing. Wang et al. (2021) used a large-eddy simulation model to assess the interplay between turbulent mixing and HONO chemistry for conditions typical of the Southeast United States and found good model-observation agreement in HONO using a $\gamma_{NO_2\rightarrow HONO}$ range of 10^{-4}–10^{-3}. Moreover, photo-sensitized heterogeneous reduction of NO_2 on organic substrates or soot particles has been observed as a major HONO source in many studies (Aubin & Abbatt, 2007; George et al., 2005; Han et al., 2016; Monge et al., 2010; Stemmler et al., 2006), especially in plumes with high NO_2 concentrations (Kleffmann et al., 1999).

Particulate nitrate (pNO_3), and surface adsorbed nitrate generally, can photolyze to produce HONO (R3), with the production rate from pNO_3 described by scaling the HNO_3(g) photolysis frequency (j_{HNO_3}) by an enhancement factor, *EnF* (Bao et al., 2018; Ye et al., 2016; Zhou et al., 2001, 2002, 2003). However, estimates of the *EnF* appear to vary with pNO_3 loading and aerosol organic composition, leading to very different conclusions as to the importance of this source (Romer et al., 2018; Ye et al., 2016, 2017). Haskins et al. (2019) reported that using an *EnF* of 300 recommended in Ye et al. (2016) overestimated measured HONO in aged wintertime urban plumes, consistent with the moderate *EnF* (1–30) reported in Romer et al. (2018) derived HNO_3/NO_x ratios. Recently, Shi et al. (2021) found the *EnF* to be <10 in laboratory experiments using suspended submicron inorganic particles.

Novel homogeneous HONO sources have also been proposed, such as the reaction between electronically excited NO_2 (NO_2^*) and H_2O (R4, S. Li et al., 2008), and the reaction between hydroperoxyl–water complex ($HO_2 \cdot H_2O$) and NO_2 (R5, X. Li et al., 2014). However, these sources are not considered atmospherically important (Amedro et al., 2011; Carr et al., 2009; Czader et al., 2012; Sörgel et al., 2011; Wong et al., 2012; Ye et al., 2015).

$$2NO_2 + H_2O(\text{surface}) \rightarrow HONO + HNO_3 \quad \text{(R1)}$$

$$NO_2 + \{R\text{–}H\}_{red}(\text{surface}) \rightarrow HONO + \{R\}_{ox} \quad \text{(R2)}$$

$$pNO_3 + h\nu \rightarrow 0.67HONO + 0.33NO_2 \quad \text{(R3)}$$

$$NO_2^* + H_2O \rightarrow HONO + OH \quad \text{(R4)}$$

$$HO_2 \cdot H_2O + NO_2 \rightarrow \alpha HONO + O_2 + H_2O \quad \text{(R5)}$$

The relative importance of different secondary HONO sources in different environments is thus not well constrained. Previous field observations show that pNO_3 photolysis is the main contributor to secondary HONO production in low-NO_x conditions such as in remote background air and forest canopy (Ye et al., 2016; Zhou et al., 2011). However, a recent isotopic analysis suggests that pNO_3 photolysis plays a minor role (<5%) while photo-enhanced NO_2-to-HONO heterogeneous conversion contributes 85%–95% to total HONO production for the aged daytime fire plume measured at the surface (Chai et al., 2021).

Wildfire plumes often are injected aloft of the well-mixed planetary boundary layer, providing an opportunity to probe the homogeneous and aerosol particle processes more directly without efficient contact with the ground surface. We use in situ airborne measurements collected during the Western Wildfire Experiment for Cloud chemistry, Aerosol absorption and Nitrogen (WE-CAN) campaign, which was carried out in summer 2018 in the western US, to examine the possible sources of HONO in aged smoke plumes aloft of the surface. We evaluate NO_2- and pNO_3-driven sources, and assess the range of key parameters associated with these sources required to

reproduce the observed HONO levels. We also apply a multinomial linear regression to determine the contributions of these pathways in wildfire smoke. We conclude with a box model simulation to show the contributions of governing secondary sources as smoke plumes age.

2. Methods

The WE-CAN campaign was based in Boise, ID, with research flights from 24 July to 31 August 2018. High time resolution measurements were conducted aboard the NCAR/NSF C-130 aircraft, including various trace gases and particulate species (such as HONO, NO_x, pNO_3, HNO_3, etc), photolysis frequencies, aerosol surface area density for submicron particles, and meteorological parameters. The details of campaign and flight descriptions can be found elsewhere (Juncosa Calahorrano et al., 2020; Lindaas et al., 2021; Palm et al., 2020; Peng et al., 2020).

HONO was measured with the University of Washington Iodide adduct Chemical Ionization Mass Spectrometer (UW I-CIMS). Details of its operation during WE-CAN and relevant calibration tests are described previously (Palm et al., 2020; Peng et al., 2020). For this analysis, we tested NO_2-to-HONO conversion in the instrument by injecting NO_2 through the inlet used during WE-CAN, and measuring HONO as a function of the NO_2 mixing ratio sampled by the inlet. A small flow (1–10 sccm) of NO_2 from a dilute calibrated cylinder (Praxair) was passed over a calcium carbonate denuder just prior to mixing with the 20 lpm inlet flow to remove HONO produced from the cylinder, regulator, flow controller, and delivery tubing surfaces. The NO_2 conversion to HONO in the inlet under WE-CAN conditions is found to be less than 0.3% (Figure S1 in Supporting Information S1) at ambient humidity. Thus, inlet NO_2-to-HONO artifacts are negligible for the WE-CAN conditions we evaluate.

We use a zero-dimensional box model, based on the Framework for 0-D Atmospheric Modeling (F0AM) to evaluate the importance of different secondary sources. Detailed descriptions for the baseline model setup have been published (Peng et al., 2021), and the application to this work is described further in the Supporting Information S1.

3. Results and Discussion

3.1. Observations of HONO Enhancement in the Far-Field

HONO is expected to reach photo-stationary steady state within a few hours downwind of fire emissions during the daytime (Peng et al., 2020). Therefore, to probe the existence of secondary HONO formation, we specifically examined wildfire smoke sampled with a physical age >3 hr during WE-CAN. During Research Flight (RF) 5, the aircraft sampled a large, merged smoke-plume originating from wildfires in California and Oregon. In this "River of Smoke," physical plume ages were above 400 min, except for a small portion of smoke possibly affected by nearby fires with 2–3 hr transport time, which are excluded from the following analysis. The minimal interference by fresh smoke intrusions makes it an ideal case study to examine the contributions of different secondary HONO sources. In addition, the plume resided in the free troposphere during sampling, which excludes complexities from ground surface interactions (Figure S2 in Supporting Information S1). We subsequently evaluate the representativeness of RF5 by comparing it to all other aged smoke sampled during WE-CAN.

Figure 1a shows satellite imagery of the wildfire smoke with RF5 flight tracks color coded and sized by 1-min average HONO mixing ratios. Active fire fronts detected by the Visible Infrared Imaging Radiometer Suite (VIIRS) thermal band are outlined in red. HONO mixing ratios were consistently enhanced in a portion of smoke intercepted in Nevada originating from fires in California. Peak HONO reached >190 ppt, well above the 3σ 1-min detection limit of ∼14 ppt (Figure 1b). Given a photolytic lifetime of 15–20 min, these HONO levels suggest an important secondary source of HONO well downwind of the emission location.

We find that HONO photolytic loss exceeds the homogeneous formation by over 10 times in the river of smoke, where OH concentrations were estimated by scaling the measured O_3 photolysis rates (Tan et al., 2019). Even at a peak OH concentration of 1×10^7 molec cm^{-3}, the reaction is still too slow, indicating the presence of an in situ HONO source.

We estimate the magnitude of missing daytime HONO source (Equation 1) from the difference between the measured HONO loss rate and homogeneous production rate. In cases of high spatial heterogeneity, this calculation

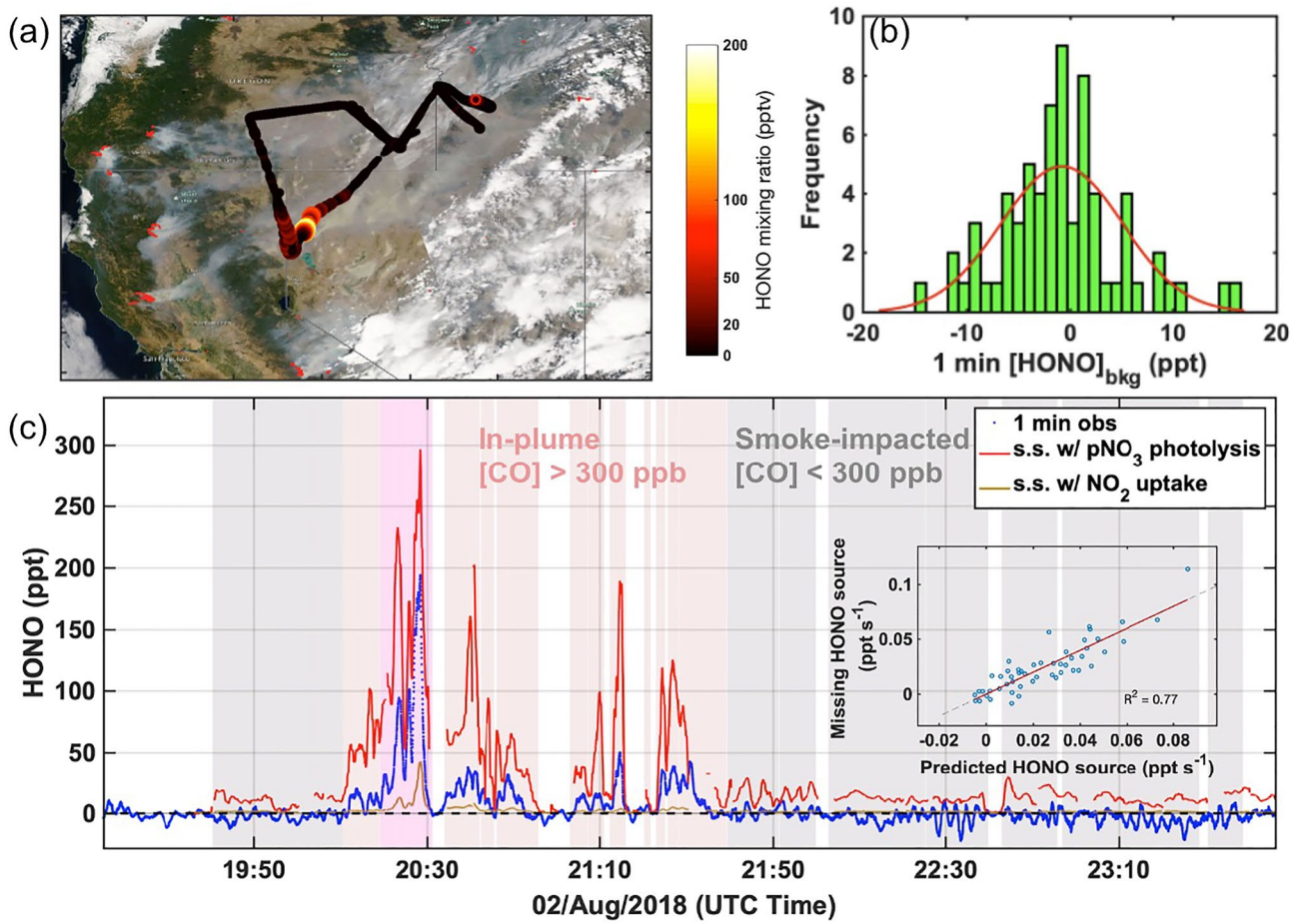

Figure 1. (a) MODIS VIIRS reflectance mapping with overlaid flight track color coded by 1-min average HONO mixing ratios (pptv) on 2 August 2018. Orange dots are active fires. (b) 1-min average HONO mixing ratios by CIMS for background air. Histogram fit: mu = −0.75 ppt, sigma = 4.6 ppt. (c) Steady state (s.s.) estimates of HONO for different potential secondary source mechanisms and observed HONO. Red shading denotes in-plume samples, magenta shading denotes measurements potentially affected by fresher plume intrusions, and gray shading denotes smoke-impacted backgrounds. The inset is the correlation between predicted HONO source strength using multilinear regression and missing HONO source strength.

may be inaccurate as the local photo-stationary state may be perturbed with changes in the composition of VOC and NO_x emissions in wildfire plumes (Crilley et al., 2016). Other sources of variability include changes in meteorological conditions as well as measurement noise. Given the short lifetime of HONO in a sunlit plume more than a few hours old and disconnected from surface deposition, we assume such changes in plume composition and meteorological conditions are minor perturbations to the plume steady state.

$$P(\mathrm{HONO})_{\mathrm{other}} = j_{\mathrm{HONO}}[\mathrm{HONO}] + k_{\mathrm{HONO+OH}}[\mathrm{HONO}][\mathrm{OH}] - k_{\mathrm{NO+OH}}[\mathrm{NO}][\mathrm{OH}] \quad (1)$$

A correlation analysis of the inferred HONO source (P_{other}) to multiple candidate mechanisms identified in the literature revealed good correlations of the inferred missing source with $p\mathrm{NO}_3$ photolysis and both dark and photo-enhanced NO_2 heterogeneous reactive uptake (Figure S3 in Supporting Information S1). We show the HONO budget time series for the River of Smoke (Figure S4 in Supporting Information S1) comparing the upper bounds of turnover rates for different NO_x-related pathways (reactions R1–R4). These NO_x-related pathways account for less than half of HONO production rates in the smoke plume in RF5 even when we applied the upper limit rate parameters from past studies.

To balance the rapid photolytic loss, we examined two plausible secondary sources based on the correlation analysis: (a) $p\mathrm{NO}_3$ photolysis; and (b) (dark and photo-enhanced) NO_2 heterogeneous reactions, using Equations 2 and 3, where $J(p\mathrm{NO}_3)$ and $J(\mathrm{HNO}_3)$ represent the photolysis frequency for $p\mathrm{NO}_3$ and HNO_3, respectively, and ω_{NO2} represents the mean molecular speed for NO_2. The correlation of an inferred HONO source from

$HO_2H_2O + NO_2$ is weak ($R^2 = 0.04$, Figure S3 in Supporting Information S1) and thus this pathway is not considered. Initially, we assume *EnF* is 300 and φ_{HONO} (HONO yield) is 0.67 (Ye et al., 2016) as the baseline for HONO production from pNO_3 photolysis (P_{pNO3}), and that $\gamma_{NO_2\rightarrow HONO}$ for HONO production on aerosol surfaces is 10^{-4}, arbitrarily the center of the range of 10^{-5} –10^{-3} derived from laboratory studies of irradiated aerosol particles (Colussi et al., 2013; Khalizov et al., 2010; Z. Liu et al., 2014; Wong et al., 2012). The measured dry surface area (S_A) has been adjusted using a hygroscopic factor following X. Liu et al. (2008) to correct for aerosol hygroscopic growth.

$$P_{pNO3} = J_{pNO3}\,[pNO_3] = EnF * \varphi_{HONO} * J_{HNO_3}\,[pNO_3] \quad (2)$$

$$P_{NO2het} = K_{het}\,[NO_2] = \frac{1}{4}\gamma_{NO2\rightarrow HONO} * \omega_{NO2} * S_A\,[NO_2] \quad (3)$$

Figure 1c shows the 1 min average observed HONO mixing ratios in RF5, as well as the steady state predicted HONO after incorporating baseline production from either of the two candidate mechanisms. The baseline pNO_3 photolysis source overestimates HONO levels by a factor of 3.2 on average, and a single *EnF* would not capture measured HONO, as the ratio of measured to predicted HONO changes across the plume intercepts. Importantly, secondary HONO formation was found to be necessary in some but not all aged plumes we sampled, as shown in Figure 1, where higher HONO levels would be expected from pNO_3 photolysis in the smoke-impacted air sampled later in time where observed HONO was effectively zero or below detection limit.

The variations of *EnF* even within one flight are substantial and may stem from differences in pNO_3 composition (e.g., organic vs. inorganic) and aerosol properties such as phase state. This cautions implementing even a modest *EnF* for HONO formation from pNO_3 photolysis in chemical-transport models. The NO_2 heterogeneous uptake alone underestimates HONO concentrations in the plumes using $\gamma_{NO2\rightarrow HONO} = 10^{-4}$. The aerosol surface area used in these calculations may be a lower limit as only submicron aerosols were measured and assessed. If NO_2 heterogeneous conversion to HONO occurs across the entire size distribution, our $\gamma_{NO2\rightarrow HONO}$ would be smaller for the same HONO production rate. As pNO_3 also likely exists in super-micron particles, the pNO_3 source is even larger than we calculate, and thus incorporating their contribution would overestimate observed HONO to an even greater extent.

3.2. Evaluation of Possible Secondary HONO Sources

Variable secondary HONO production may stem from different chemical and physical conditions in the plume. Multiple production pathways could also co-exist with relative contributions varying with plume age and smoke conditions. To further elucidate the relative importance of these processes as HONO sources, we performed a multinomial linear regression analysis of the unknown HONO source with baseline production mechanisms in Section 3.1 as variables (Equation 4).

$$P_{unknown} = a + b * P_{pNO3} + c * P_{NO2het} \quad (4)$$

Parameters b and c are scaling factors of the corresponding baseline HONO source terms in Equations 2 and 3 and parameter a denotes the residual. The optimal fit parameters for the River of Smoke (RF5) are $a = -0.008$ (-0.014, -0.0016), $b = 0.21$ (0.12, 0.30) and $c = 4.9$ (2.2, 7.6), where values in parentheses are the interquartile range. These values translate to an *EnF* of 63, and $\gamma_{NO2\rightarrow HONO}$ of 4.9×10^{-4}. The correlation of fitted HONO secondary source with the missing HONO source strength is shown in Figure 1c inset ($R^2 = 0.77$). These results suggest a factor of ~5 smaller HONO source from pNO_3 photolysis in wildfire smoke than reported by Ye et al. (2018), but a significant source of HONO from NO_2 reactive uptake to aerosol particles, and an important role of smoke particles as a media for secondary HONO chemistry, in contrast to previous conclusions that aerosols are not important in daytime HONO production (Ammann et al., 1998; Bröske et al., 2003; K. Stemmler et al., 2007; Vandenboer et al., 2013; Wong et al., 2011).

We studied smoke plumes intercepted in all flights with physical ages above 3 hr, and the overall statistics are presented in Table S1 in Supporting Information S1. Significant enhancements in HONO mixing ratios, with a median value of ~56 ppt across the campaign, were observed in these aged wildfire plumes compared to background air masses. The campaign-average missing HONO source strength (0.029 ± 0.039 ppt s^{-1}) is comparable

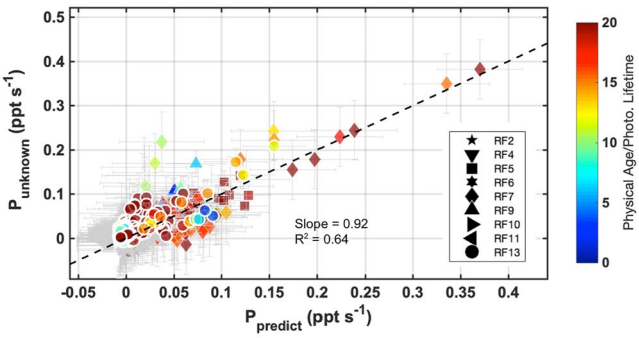

Figure 2. Scatter plot of the inferred HONO source strength ($P_{unknown}$) against that predicted from multilinear regression ($P_{predict}$) using River of Smoke parameters. Each point represents a 1-min average and is colored by the ratio of plume physical age to HONO photolysis lifetime. The error bars represent the uncertainties from the regression coefficients. A 1:1 line (black dashed) is shown for reference. The R^2 value for the least squares fit for the scatter plot was 0.64.

to those obtained from aircraft studies in Michigan (0.016 ppt s^{-1}; N. Zhang et al., 2009) and in the southern USA (0.047 ppt s^{-1}; Ye et al., 2018), while much smaller than over the North China Plain in winter and spring (0.13 and 0.18 ppt s^{-1}; Jiang et al., 2020). We find a dependence of missing HONO source strength on both candidate mechanisms in aged wildfire smoke across flights (Figure S5 in Supporting Information S1).

In Figure 2, we show the ability of Equation 4 with fit parameters acquired from the River of Smoke (RF5) to explain missing HONO production in aged smoke in all other flights. The symbols are colored by the effective aging metric (physical age to photolysis lifetime) which accounts for the difference in photolysis due to varying light conditions. The predicted secondary HONO production rates have overall good correlation with the inferred missing source rate (R^2 of 0.64, slope = 0.92). These results suggest that a combination of NO_2-driven and pNO_3-driven HONO sources can explain a majority of the missing HONO source strength, with relatively consistent weighting across different fires. The variance may be partially due to changes in the rate coefficients from both pathways with chemical composition in different smoke intercepts (Z. Liu et al., 2014; Ye et al., 2017; W. Zhang et al., 2020), and uncertainties or variations in the photolysis lifetime over the age of a plume. Meanwhile, other HONO sources like photolysis of ortho-nitrophenols (Bejan et al., 2006) and the contribution of super-micron particles are not ruled out, and as such *EnF* and $\gamma_{NO2\rightarrow HONO}$ presented here are likely upper limits.

3.3. Contributions of Secondary HONO Across Multiple Fires

In Figure 3, we derive an upper limit estimate of the magnitude of pNO_3 photolysis and NO_2 reactive uptake sources of HONO using aged smoke plume intercepts from all flights. Assuming each source is exclusive, the median and interquartile range of the parameter distribution across all flights are estimated to be $b = 0.40$ (0.22, 0.70) and $c = 9.8$ (4.6, 21.0), which in turn suggest the median upper-limit value for NO_2 uptake is 10–1,000 times higher than reported in other field studies (Z. Liu et al., 2014; W. Zhang et al., 2020). This higher $\gamma_{NO2\rightarrow HONO}$ value may suggest that a more efficient heterogeneous conversion from NO_2 to HONO is present in aged fire smoke, but its importance is strongly influenced by the assumed magnitude of the pNO_3 photolysis source. Figure 3c shows that if both sources contribute, the c values start to become negative for $b \geq 0.2$ for certain flights, and the variations in c are small despite orders of magnitude changes in b reflecting a relatively narrow range for $\gamma_{NO_2\rightarrow HONO}$, on the order of 10^{-4}, and a lower photolysis rate of pNO_3 in fire smoke than reported in Ye et al. (2016). As noted above, variations in these parameters may arise from aerosol particle properties, for example, pH, water content, and organic nitrate to inorganic nitrate fraction, among others. The fraction of total particulate nitrate that is inorganic nitrate in wildfire smoke may add uncertainty to our conclusions, though previous box modeling of WE-CAN plumes suggest total fine mode nitrate can be explained with mostly inorganic nitrate in the near field (Peng et al., 2021).

In Figure 4, we compare direct HONO emissions to the secondary HONO sources evaluated above using simulations of the evolution of two fire plumes where in situ plume sampling included a sequence of downwind cross-plume intercepts. Adding secondary HONO sources to the F0AM model (Peng et al., 2021) improved HONO simulations compared to observations especially in the older plume portions. pNO_3 photolysis becomes more important with aging and more predominant in less polluted events (i.e., lower NO_x loading), while NO_2-related reactions and homogeneous HONO formation are more important in early, higher NO_x stages of the plume. Model simulations for other compounds are shown in Figure S6 in Supporting Information S1. We neglect uptake of HONO to aerosol (Figure S7 in Supporting Information S1), we assume particulate organic nitrates are a minor fraction of measured particulate nitrate (Figure S8 in Supporting Information S1), and we use measured j_{HONO} as a function of plume age (Figure S9 in Supporting Information S1). The formation of HNO_3 from NO_2 heterogeneous uptake has a negligible impact on the predicted total nitrate. Secondary HONO sources are negligible for young plumes (age <1h) compared to primary emissions, accounting for <4% of measured HONO while

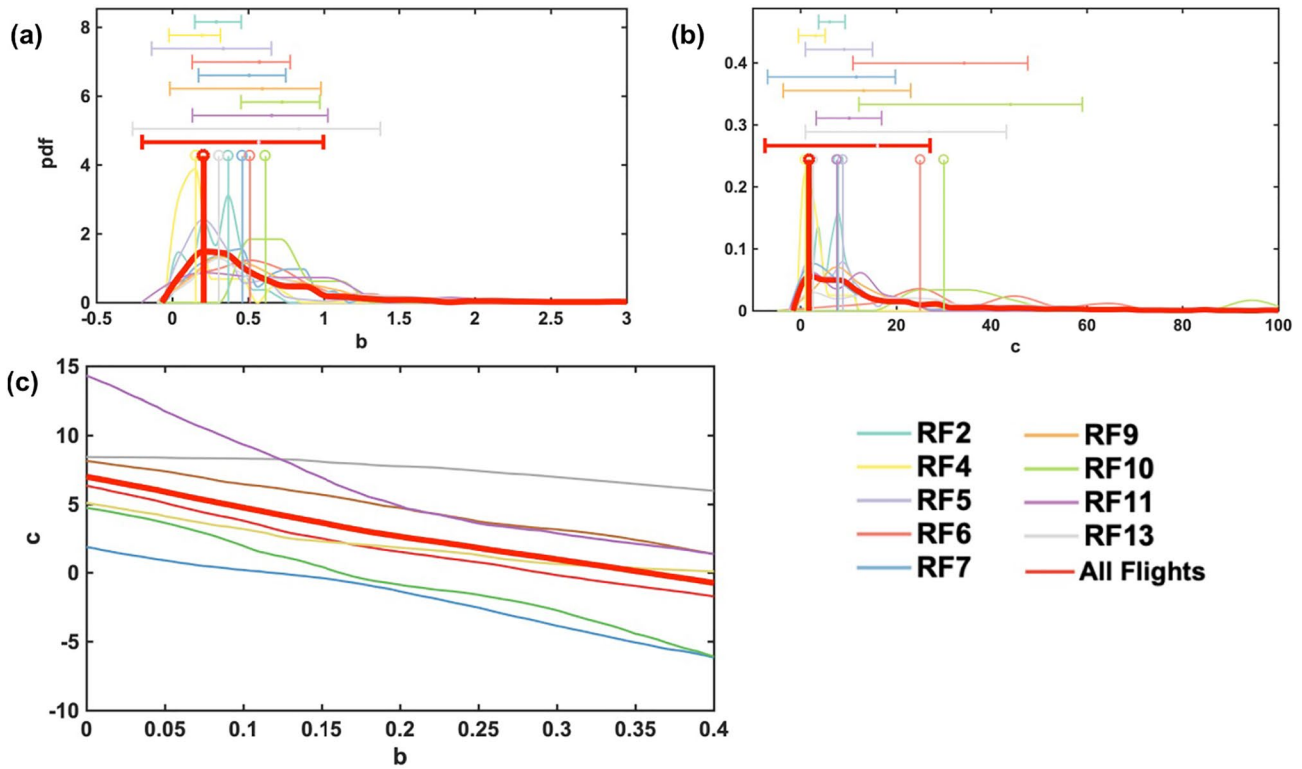

Figure 3. Histograms of weight coefficients (a) *b* and (b) *c* for the multilinear fit of HONO secondary sources for different flights ($P_{\text{unknown}} = a + b * P_{p\text{NO3}} + c * P_{\text{NO2het}}$) assuming each source is exclusive. The all-flight average distribution is shown in thick red. Vertical lines indicate the mode value for each flight. Overhead error bars denote mean ± standard deviation for each flight. The median and interquartile range is 0.40 and (0.22,0.70) for b, and 9.8 and (4.6, 21.0) for (c) (c) Variations of c with increasing b assuming both sources contribute to HONO production. Each curve represents one flight and the red curve denotes the median of all flights.

making up >90% of the HONO source in plumes >2h old. The integral of secondary HONO production over the full model simulation for the Taylor Creek Fire is ∼2 ppb, while the initial HONO from direct emissions is ∼72 ppb, suggesting that the secondary HONO formation is only a small contribution to HONO in the fire smoke overall in the first ∼ day of aging.

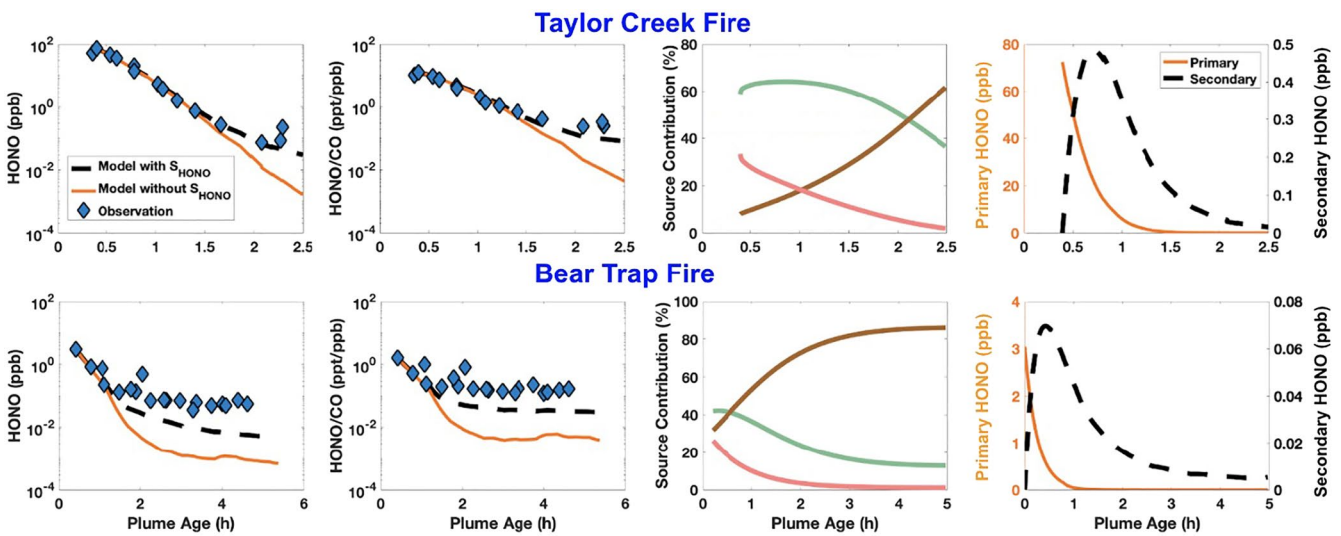

Figure 4. Box model simulations with (dashed black lines) and without (solid orange lines) secondary HONO sources (S_{HONO}) for Taylor Creek Fire (RF3, top) and Bear Trap Fire (RF9, bottom). NO_2 uptake to aerosol (green line, third panel from left) exceeds pNO_3 photolysis (brown line, third panel from the left) as a source of HONO in the early stages of the Taylor Creek Fire, but in the Bear Trap Fire and more aged plumes pNO_3 photolysis is more important.

4. Conclusions

We provide direct constraints on the production of secondary HONO in daytime wildfire smoke using in situ airborne measurements collected over the western US We find that the dominant secondary sources of HONO in aged fire smoke are NO_2 reactive uptake and pNO_3 photolysis. These findings highlight the potential importance of biomass burning aerosols as a media for secondary HONO production. A simple multi-linear regression model derived from a case study of aged smoke from major wildfires in California and Oregon was found to explain 64% of the variance in missing HONO production in all aged smoke detected during the WE-CAN campaign. A median *EnF* of 63 for pNO_3 photolysis frequency relative to HNO_3 and $\gamma_{NO_2 \rightarrow HONO}$ of 4.9×10^{-4} extend to all fire plumes sampled in WE-CAN. Box model simulations with additional secondary HONO mechanisms improve the model-observation agreement in HONO, especially for more aged plumes, while finding that secondary HONO is a small OH source compared to the primary HONO in the first day of aging. Our observations are unique in extending previous studies of HONO sources to wildfire plumes decoupled from the ground, and offer a range of key parameters, which constrain estimates of oxidation rates in biomass burning plumes.

Data Availability Statement

All data used in this paper are collected during the WE-CAN campaign in 2018 and are publicly available. The merged data set (version 4) is managed by NCAR's Earth Observing Laboratory and could be downloaded at https://www-air.larc.nasa.gov/cgi-bin/ArcView/firexaq?MERGE=1. Modeling data and plume transect observations across different fires can be downloaded in the open science framework https://osf.io/ncs52/.

Acknowledgments
The research was supported by the National Science Foundation (Grant NSF-AGS 1652688,1650786, 1650275) and National Oceanic and Atmospheric Administration (NOAA Grant NA17OAR4310012). The authors thank all those who helped organize and participated in the 2018 WE-CAN campaign. This material is based upon work supported by the National Center for Atmospheric Research, which is a major facility sponsored by the National Science Foundation under Cooperative Agreement No. 1852977. The data were collected using NSF's Lower Atmosphere Observing Facilities, which are managed and operated by NCAR's Earth Observing Laboratory. The operational and scientific support from NCAR's Earth Observing Laboratory and Research Aircraft Facility is gratefully acknowledged.

References

Acker, K., Spindler, G., & Brüggemann, E. (2004). Nitrous and nitric acid measurements during the INTERCOMP2000 campaign in Melpitz. *Atmospheric Environment*, *38*(38), 6497–6505. https://doi.org/10.1016/J.ATMOSENV.2004.08.030

Amedro, D., Parker, A. E., Schoemaecker, C., & Fittschen, C. (2011). Direct observation of OH radicals after 565 nm multi-photon excitation of NO_2 in the presence of H_2O. *Chemical Physics Letters*, *1–3*(513), 12–16. https://doi.org/10.1016/J.CPLETT.2011.07.062

Ammann, M., Kalberer, M., Jost, D. T., Tobler, L., Rössler, E., Piguet, D., et al. (1998). Heterogeneous production of nitrous acid on soot in polluted air masses. *Nature*, *395*(6698), 157–160. https://doi.org/10.1038/25965

Aubin, D. G., & Abbatt, J. P. D. (2007). Interaction of NO_2 with hydrocarbon soot: Focus on HONO yield, surface modification, and mechanism. *The Journal of Physical Chemistry. A*, *111*(28), 6263–6273. https://doi.org/10.1021/JP068884H

Bao, F., Li, M., Zhang, Y., Chen, C., & Zhao, J. (2018). Photochemical aging of Beijing urban PM2.5: HONO production. *Environmental Science and Technology*, *52*(11), 6309–6316. https://doi.org/10.1021/ACS.EST.8B00538

Bejan, I., Abd El Aal, Y., Barnes, I., Benter, T., Bohn, B., Wiesen, P., & Kleffmann, J. (2006). The photolysis of ortho-nitrophenols: A new gas phase source of HONO. *Physical Chemistry Chemical Physics*, *8*(17), 2028–2035. https://doi.org/10.1039/B516590C

Bröske, R., Kleffmann, J., & Wiesen, P. (2003). Atmospheric chemistry and physics. *European Geosciences Union*, *3*(3), 469–474. https://doi.org/10.5194/acp-3-469-2003

Carr, S., Heard, D. E., & Blitz, M. A. (2009). Comment on "atmospheric hydroxyl radical production from electronically excited NO_2 and H_2O". *Science*, *324*(5925), 336. https://doi.org/10.1126/SCIENCE.1166669

Chai, J., Dibb, J. E., Anderson, B. E., Bekker, C., Blum, D. E., Heim, E., et al. (2021). Isotopic evidence for dominant secondary production of HONO in near-ground wildfire plumes. *Atmospheric Chemistry and Physics*, *21*(17), 13077–13098. https://doi.org/10.5194/ACP-21-13077-2021

Colussi, A. J., Enami, S., Yabushita, A., Hoffmann, M. R., Liu, W. G., Mishra, H., & Goddard, W. A. (2013). Tropospheric aerosol as a reactive intermediate. *Faraday Discussions*, *165*(0), 407–420. https://doi.org/10.1039/C3FD00040K

Crilley, L. R., Louisa Kramer, D., Pope, F. K., Whalley, L. R., Cryer, D. E., Heard, D., et al. (2016). On the interpretation of in situ HONO observations via photochemical steady state. *Faraday Discussions*, *189*(0), 191–212. https://doi.org/10.1039/C5FD00224A

Czader, B. H., Rappengï Uck, B., Percell, P., Byun, D. W., Ngan, F., & Kim, S. (2012). Modeling nitrous acid and its impact on ozone and hydroxyl radical during the Texas Air Quality Study 2006. *Atmospheric Chemistry and Physics*, *12*(15), 6939–6951. https://doi.org/10.5194/acp-12-6939-2012

Finlayson-Pitts, B. J., Wingen, L. M., Sumner, A. L., Syomin, D., & Ramazan, K. A. (2003). The heterogeneous hydrolysis of NO_2 in laboratory systems and in outdoor and indoor atmospheres: An integrated mechanism. *Physical Chemistry Chemical Physics*, *5*(2), 223–242. https://doi.org/10.1039/B208564J

George, C., Strekowski, R. S., Kleffmann, J., Stemmler, K., & Ammann, M. (2005). Photoenhanced uptake of gaseous NO_2 on solid organic compounds: A photochemical source of HONO? *Faraday Discussions*, *130*(0), 195–210. https://doi.org/10.1039/B417888M

Gustafsson, R. J., Kyriakou, G., & Lambert, R. M. (2008). The molecular mechanism of tropospheric nitrous acid production on mineral dust surfaces. *ChemPhysChem : A European Journal of Chemical Physics and Physical Chemistry*, *9*(10), 1390–1393. https://doi.org/10.1002/CPHC.200800259

Han, C., Yang, W., Wu, Q., Yang, H., & Xue, X. (2016). Heterogeneous photochemical conversion of NO_2 to HONO on the humic acid surface under simulated sunlight. *Environmental Science and Technology*, *50*(10), 5017–5023. https://doi.org/10.1021/ACS.EST.5B05101

Haskins, J. D., Lopez-Hilfiker, F. D., Lee, B. H., Shah, V., Wolfe, G. M., DiGangi, J., et al. (2019). Anthropogenic control over wintertime oxidation of atmospheric pollutants. *Geophysical Research Letters*, *46*(24), 14826–14835. https://doi.org/10.1029/2019GL085498

Jiang, Y., Xue, L., Gu, R., Jia, M., Zhang, Y., Wen, L., et al. (2020). Sources of nitrous acid (HONO) in the upper boundary layer and lower free troposphere of the North China Plain: Insights from the Mount Tai Observatory. *Atmospheric Chemistry and Physics*, *20*(20), 12115–12131. https://doi.org/10.5194/ACP-20-12115-2020

Juncosa Calahorrano, J. F., Lindaas, J., O'Dell, K., Palm, B. B., Peng, Q., Flocke, F., et al. (2020). Daytime oxidized reactive nitrogen partitioning in Western U.S. wildfire smoke plumes. *Journal of Geophysical Research: Atmospheres*, *126*(4), e2020JD033484. https://doi.org/10.1029/2020JD033484

Khalizov, A. F., Cruz-Quinones, M., & Zhang, R. (2010). Heterogeneous reaction of NO_2 on fresh and coated soot surfaces. *Journal of Physical Chemistry A*, *114*(28), 7516–7524. https://doi.org/10.1021/jp1021938

Kleffmann, J., Becker, K. H., Lackhoff, M., & Wiesen, P. (1999). Heterogeneous conversion of NO_2 on carbonaceous surfaces. *Physical Chemistry Chemical Physics*, *1*(24), 5443–5450. https://doi.org/10.1039/A905545B

Lee, B. H., Wood, E. C., Herndon, S. C., Lefer, B. L., Luke, W. T., Brune, W. H., et al. (2013). Urban measurements of atmospheric nitrous acid: A caveat on the interpretation of the HONO photostationary state. *Journal of Geophysical Research: Atmospheres*, *118*(21), 12274–12281. https://doi.org/10.1002/2013JD020341

Li, S., Matthews, J., & Sinha, A. (2008). Atmospheric hydroxyl radical production from electronically excited NO_2 and H_2O. *Science*, *319*(5870), 1657–1660. https://doi.org/10.1126/SCIENCE.1151443

Li, X., Rohrer, F., Hofzumahaus, A., Brauers, T., Häseler, R., Bohn, B., et al. (2014). Missing gas-phase source of HONO inferred from Zeppelin measurements in the troposphere. *Science*, *344*(6181), 292–296. https://doi.org/10.1126/SCIENCE.1248999

Lindaas, J., Pollack, I. B., Garofalo, L. A., Pothier, M. A., Farmer, D. K., Kreidenweis, S. M., et al. (2021). Emissions of reactive nitrogen from Western U.S. wildfires during summer 2018. *Journal of Geophysical Research: Atmospheres*, *126*(2), e2020JD032657. https://doi.org/10.1029/2020JD032657

Liu, X., Cheng, Y., Zhang, Y., Jung, J., Sugimoto, N., Chang, S. Y., et al. (2008). Influences of relative humidity and particle chemical composition on aerosol scattering properties during the 2006 PRD campaign. *Atmospheric Environment*, *42*(7), 1525–1536. https://doi.org/10.1016/J.ATMOSENV.2007.10.077

Liu, Z., Wang, Y., Costabile, F., Amoroso, A., Zhao, C., Greg Huey, L., et al. (2014). Evidence of aerosols as a media for rapid daytime HONO production over China. https://doi.org/10.1021/es504163z

Monge, M. E., D'Anna, B., Mazri, L., Giroir-Fendler, A., Ammann, M., Donaldson, D. J., & George, C. (2010). Light changes the atmospheric reactivity of soot. *Proceedings of the National Academy of Sciences*, *107*(15), 6605–6609. https://doi.org/10.1073/PNAS.0908341107

Neuman, J. A., Trainer, M., Brown, S. S., Min, K.-E., Nowak, J. B., Parrish, D. D., et al. (2016). HONO emission and production determined from airborne measurements over the Southeast U.S. *Journal of Geophysical Research: Atmospheres*, *121*(15), 9237–9250. https://doi.org/10.1002/2016JD025197

Palm, B. B., Peng, Q., Fredrickson, C. D., Lee, B. H., Garofalo, L. A., Pothier, M. A., et al. (2020). Quantification of organic aerosol and brown carbon evolution in fresh wildfire plumes. *Proceedings of the National Academy of Sciences of the United States of America*, *117*(47), 29469–29477. https://doi.org/10.1073/pnas.2012218117

Peng, Q., Palm, B. B., Fredrickson, C. D., Lee, B. H., Hall, S. R., Ullmann, K., et al. (2021). Observations and modeling of NO_x photochemistry and fate in fresh wildfire plumes. *ACS Earth and Space Chemistry*, *5*(10), 2652–2667. https://doi.org/10.1021/ACSEARTHSPACECHEM.1C00086

Peng, Q., Palm, B. B., Melander, K. E., Lee, B. H., Hall, S. R., Ullmann, K., et al. (2020). HONO emissions from Western U.S. wildfires provide dominant radical source in fresh wildfire smoke. *Environmental Science and Technology*, *54*(10), 5954–5963. https://doi.org/10.1021/acs.est.0c00126

Romer, P. S., Wooldridge, P. J., Crounse, J. D., Kim, M. J., Wennberg, P. O., Dibb, J. E., et al. (2018). Constraints on aerosol nitrate photolysis as a potential source of HONO and NO_x. *Environmental Science and Technology*, *52*(23), 13738–13746. https://doi.org/10.1021/acs.est.8b03861

Shi, Q., Tao, Y., Krechmer, J. E., Heald, C. L., Murphy, J. G., Kroll, J. H., & Ye, Q. (2021). Laboratory investigation of renoxification from the photolysis of inorganic particulate nitrate. *Environmental Science and Technology*, *55*(2), 854–861. https://doi.org/10.1021/ACS.EST.0C06049

Sörgel, M., Trebs, I., Serafimovich, A., Moravek, A., Held, A., & Zetzsch, C. (2011). Simultaneous HONO measurements in and above a forest canopy: Influence of turbulent exchange on mixing ratio differences. *Atmospheric Chemistry and Physics*, *11*(2), 841–855. https://doi.org/10.5194/ACP-11-841-2011

Stemmler, K., Ammann, M., Donders, C., Kleffmann, J., & George, C. (2006). Photosensitized reduction of nitrogen dioxide on humic acid as a source of nitrous acid. *Nature*, *440*(7081), 195–198. https://doi.org/10.1038/nature04603

Stemmler, K., Ndour, M., Elshorbany, Y., Kleffmann, J., D'Anna, B., George, C., et al. (2007). Light induced conversion of nitrogen dioxide into nitrous acid on submicron humic acid aerosol. *Atmospheric Chemistry and Physics*, *7*(16), 4237–4248. https://doi.org/10.5194/acp-7-4237-2007

Tan, Z., Lu, K., Hofzumahaus, A., Fuchs, H., Bohn, B., Holland, F., et al. (2019). Experimental budgets of OH, HO_2, and RO_2 radicals and implications for ozone formation in the Pearl River Delta in China 2014. *Atmospheric Chemistry and Physics*, *19*(10), 7129–7150. https://doi.org/10.5194/acp-19-7129-2019

Vandenboer, T. C., Brown, S. S., Murphy, J. G., Keene, W. C., Young, C. J., Pszenny, A. A. P., et al. (2013). Understanding the role of the ground surface in HONO vertical structure: High resolution vertical profiles during NACHTT-11. *Journal of Geophysical Research: Atmospheres*, *118*(17), 10155–10171. https://doi.org/10.1002/JGRD.50721

Veres, P. R., Roberts, J. M., Wild, R. J., Edwards, P. M., Brown, S. S., Bates, T. S., et al. (2015). Peroxynitric acid (HO_2 NO_2) measurements during the UBWOS 2013 and 2014 studies using iodide ion chemical ionization mass spectrometry. *Atmospheric Chemistry and Physics*, *15*(14), 8101–8114. https://doi.org/10.5194/acp-15-8101-2015

Wang, S., Coggon, M. M., Gkatzelis, G. I., Warneke, C., Bourgeois, I., Ryerson, T., et al. (2021). Chemical tomography in a fresh wildland fire plume: A large eddy simulation (LES) study. *Journal of Geophysical Research: Atmospheres*, *126*(18). https://doi.org/10.1029/2021JD035203

WE-CAN Science Team. (2018). Western wildfire experiment for cloud chemistry, aerosol absorption and nitrogen field campaign data (version 4). [Dataset]. WECAN. Retrieved from https://www-air.larc.nasa.gov/cgi-bin/ArcView/firexaq?MERGE=1

Wong, K. W., Lefer, B. L., Rappenglück, B., & Stutz, J. (2011). Vertical profiles of nitrous acid in the nocturnal urban atmosphere of Houston, TX. *Atmospheric Chemistry and Physics*, *11*(8), 3595–3609. https://doi.org/10.5194/ACP-11-3595-2011

Wong, K. W., Tsai, C., Lefer, B., Haman, C., Grossberg, N., Brune, W. H., et al. (2012). Daytime HONO vertical gradients during SHARP 2009 in Houston, TX. *Atmospheric Chemistry and Physics*, *12*(2), 635–652. https://doi.org/10.5194/ACP-12-635-2012

Ye, C., Zhang, N., Gao, H., & Zhou, X. (2017). Photolysis of particulate nitrate as a source of HONO and NOx. *Environmental Science and Technology*, *51*(12), 6849–6856. https://doi.org/10.1021/ACS.EST.7B00387

Ye, C., Zhou, X., Pu, D., Stutz, J., Festa, J., Spolaor, M., et al. (2015). Comment on "Missing gas-phase source of HONO inferred from Zeppelin measurements in the troposphere". *Science*, *348*(6241), 1326d. https://doi.org/10.1126/SCIENCE.AAA1992

Ye, C., Zhou, X., Pu, D., Stutz, J., Festa, J., Spolaor, M., et al. (2016). Rapid cycling of reactive nitrogen in the marine boundary layer. *Nature*, *532*(7600), 489–491. https://doi.org/10.1038/nature17195

Ye, C., Zhou, X., Pu, D., Stutz, J., Festa, J., Spolaor, M., et al. (2018). Tropospheric HONO distribution and chemistry in the southeastern US. *Atmospheric Chemistry and Physics*, *18*(12), 9107–9120. https://doi.org/10.5194/acp-18-9107-2018

Zhang, N., Zhou, X., Shepson, P. B., Gao, H., Alaghmand, M., & Stirm, B. (2009). Aircraft measurement of HONO vertical profiles over a forested region. *Geophysical Research Letters*, *36*(15). https://doi.org/10.1029/2009GL038999

Zhang, W., Tong, S., Jia, C., Wang, L., Liu, B., Tang, G., et al. (2020). Different HONO sources for three layers at the urban area of Beijing. *Environmental Science and Technology*, *54*(20), 12870–12880. https://doi.org/10.1021/ACS.EST.0C02146

Zhou, X., Beine, H. J., Honrath, R. E., Fuentes, J. D., Simpson, W., Shepson, P. B., & Bottenheim, J. W. (2001). Snowpack photochemical production of HONO: A major source of OH in the Arctic boundary layer in springtime. *Geophysical Research Letters*, *28*(21), 4087–4090. https://doi.org/10.1029/2001GL013531

Zhou, X., Gao, H., He, Y., Huang, G., Bertman, S. B., Civerolo, K., & Schwab, J. (2003). Nitric acid photolysis on surfaces in low-NO_x environments: Significant atmospheric implications. *Geophysical Research Letters*, *30*(23), 2217. https://doi.org/10.1029/2003GL018620

Zhou, X., He, Y., Huang, G., Thornberry, T. D., Carroll, M. A., & Bertman, S. B. (2002). Photochemical production of nitrous acid on glass sample manifold surface. *Geophysical Research Letters*, *29*(14), 26-1–26-4. https://doi.org/10.1029/2002GL015080

Zhou, X., Zhang, N., Teravest, M., Tang, D., Hou, J., Bertman, S., et al. (2011). Nitric acid photolysis on forest canopy surface as a source for tropospheric nitrous acid. *Nature Geoscience*, *29*(7), 440–443. https://doi.org/10.1038/NGEO1164

References From the Supporting Information

Brock, C. A., Williamson, C., Kupc, A., Froyd, K. D., Erdesz, F., Wagner, N., et al. (2019). Aerosol size distributions during the Atmospheric Tomography Mission (ATom): Methods, uncertainties, and data products. *Atmospheric Measurement Techniques*, *12*(6), 3081–3099. https://doi.org/10.5194/AMT-12-3081-2019

Garofalo, L. A., Pothier, M. A., Levin, E. J. T., Campos, T., Kreidenweis, S. M., & Farmer, D. K. (2019). Emission and evolution of submicron organic aerosol in smoke from wildfires in the Western United States. *ACS Earth and Space Chemistry*, *3*(7), 1237–1247. https://doi.org/10.1021/acsearthspacechem.9b00125

Marquardt, E. T. (1975). Student response to assignments requiring participation. *Improving College and University Teaching*, *23*(2), 82–83. https://doi.org/10.1080/00193089.1975.9927250

Ridley, B. A., & Grahek, F. E. (1990). A small, low flow, high sensitivity reaction Vvssel for NO chemiluminescence detectors. *Journal of Atmospheric and Oceanic Technology*, *7*(2), 307–311. https://doi.org/10.1175/1520-0426(1990)007<0307:aslfhs>2.0.co;2

Shetter, R. E., & Müller, M. (1999). Photolysis frequency measurements using actinic flux spectroradiometry during the PEM-Tropics mission: Instrumentation description and some results. *Journal of Geophysical Research*, *104*(D5), 5647–5661. https://doi.org/10.1029/98JD01381